



**HAL**  
open science

## On the control of spin flop in synthetic antiferromagnetic films

B. Negulescu, Daniel Lacour, M. Hehn, A. Gerken, J. Paul, C. Duret

► **To cite this version:**

B. Negulescu, Daniel Lacour, M. Hehn, A. Gerken, J. Paul, et al.. On the control of spin flop in synthetic antiferromagnetic films. *Journal of Applied Physics*, 2011, 109 (10), pp.103911. 10.1063/1.3583584 . hal-01741526

**HAL Id: hal-01741526**

**<https://hal.science/hal-01741526v1>**

Submitted on 21 Aug 2024

**HAL** is a multi-disciplinary open access archive for the deposit and dissemination of scientific research documents, whether they are published or not. The documents may come from teaching and research institutions in France or abroad, or from public or private research centers.

L'archive ouverte pluridisciplinaire **HAL**, est destinée au dépôt et à la diffusion de documents scientifiques de niveau recherche, publiés ou non, émanant des établissements d'enseignement et de recherche français ou étrangers, des laboratoires publics ou privés.

RESEARCH ARTICLE | MAY 23 2011

# On the control of spin flop in synthetic antiferromagnetic films


B. Negulescu; D. Lacour; M. Hehn; A. Gerken; J. Paul; C. Duret


 Check for updates


*J. Appl. Phys.* 109, 103911 (2011)


<https://doi.org/10.1063/1.3583584>




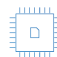
 Nanotechnology & Materials Science


 Optics & Photonics

 Impedance Analysis

 Scanning Probe Microscopy

 Sensors

 Failure Analysis & Semiconductors




## Unlock the Full Spectrum.

From DC to 8.5 GHz.

Your Application. Measured.

[Find out more](#)



## On the control of spin flop in synthetic antiferromagnetic films

B. Negulescu,<sup>1,a)</sup> D. Lacour,<sup>1</sup> M. Hehn,<sup>1</sup> A. Gerken,<sup>2</sup> J. Paul,<sup>2</sup> and C. Duret<sup>3</sup>

<sup>1</sup>*Institut Jean Lamour, CNRS, Nancy-Université, BP 70239, F-54506 Vandœuvre lès Nancy, France*

<sup>2</sup>*Sensitec GmbH, 55131 Mainz, Germany*

<sup>3</sup>*SNR Roulements, 74010 Annecy, France*

(Received 9 February 2011; accepted 27 March 2011; published online 23 May 2011)

The paper presents a systematic study of anneal induced anisotropies in a CoFe/Ru/CoFe synthetic antiferromagnet (SAF) exchange coupled with an IrMn film. When the annealing is done with the SAF in a spin flop state, the magnetic layers can be pinned perpendicular to the annealing field direction. The main parameters controlling this process are identified and analyzed: the value and the direction of the annealing field along with the Ruderman-Kittel-Kasuya-Yosida coupling energy between the two ferromagnetic layers. The induced anisotropy is predicted within a theoretical model taking into account the thermal variation of the coupling constants. Finally, the spin flop annealing is used to orthogonally pin the reference and the detection electrodes in an IrMn/CoFe/Ru/CoFe/Cu/CoFe/IrMn spin valve structure. The magnetoresistance variation in this structure is analyzed as a function of the pinning direction of the SAF acquired during the annealing in the spin flop state. A very good agreement is observed between the experimental and theoretically predicted responses. © 2011 American Institute of Physics. [doi:10.1063/1.3583584]

### I. INTRODUCTION

A synthetic antiferromagnet (SAF) consists of two ferromagnetic (F) layers antiparallely (AP) coupled via a thin metallic nonmagnetic layer. With its closed magnetic flux configuration in the ground state, the SAF provides the advantage of reduced magnetostatic interactions between the electrodes of magnetoresistive devices that is interesting for many spintronics applications.<sup>1,2</sup> The magnetic orientation of this structure is, however, instable at quite low field values.<sup>3–5</sup> Indeed, the magnetic moments of a SAF can flop in a field applied parallel to the layers, which is similar to the spin flop (SF) phenomenon in an antiferromagnetic (AF) material. This instability can be removed by pinning one of the F layers of the SAF structure with a natural AF.<sup>4</sup> More recently, the spin flop effect in SAFs was used in order to induce crossed anisotropies in the devices where not only the reference layer is exchange coupled with an AF film, but also the sensing layer.<sup>6,7</sup> The method consists of controlling the exchange anisotropy direction of the SAF by pinning it in a spin flop state, while the magnetization of the bilayer detection electrode is frozen in the direction of the annealing field. The anisotropy in the soft layer of a magnetoresistive (MR) sensor is required in order to avoid the Barkhausen noise during the magnetization reversal. While the standard approach in the hard disk read head is the use of shape anisotropy and hard magnet tail stabilization schemes,<sup>8</sup> the exchange pinning of the soft electrode provides the advantage of simplifying the patterning process and allows easy control over the sensitivity of the sensor as shown in our previous study.<sup>9</sup>

If the structure is deposited under a magnetic field, the exchange anisotropy can be set directly during the deposition

process. In this case, the parameters controlling the spin flop effect are the thicknesses of the SAF layers.<sup>10–13</sup> Another approach consists of annealing the samples under the specific field values that ensure the magnetization flop.<sup>6</sup> A phenomenological macrospin model is generally used to analyze the reversal of the F layers and to estimate the flop angle of the magnetization. When the spin flop is tuned by the thickness control, this model reproduces the experimental results quite well.<sup>11,12</sup> However, when the exchange anisotropy is established by spin flop annealing, a model taking the temperature variation of the anisotropy constants into account should be considered.

In this paper we focus on the control of spin flop annealing of a CoFe/Ru/CoFe/IrMn multilayer. Combining vibrating sample magnetometry and magnetic force microscopy (MFM), we investigate the anisotropy of the system before and after different annealing procedures. The experimental results are analyzed in the framework of a macrospin model, taking into account the temperature variation for the main parameters. In this way we are able to predict the spin flop angles as a function of the annealing field and temperature. Finally, to test the predictive capacity of the model, we have fabricated GMR based magnetic sensors using the spin flop annealing procedure. Their linear magnetoresistive responses are in very good agreement with the responses predicted by the model.

### II. RESULTS AND DISCUSSIONS

The spin flop annealing process is studied on pinned SAF samples having the following structure: buffer/IrMn(7)/CoFe(1.5)/Ru(0.8)/CoFe(2.5)/top (the thicknesses in brackets are indicated in nm). The structures are deposited in a DC magnetron sputtering tool with a base pressure of  $2 \times 10^{-8}$  Torr. No magnetic field is applied during the deposition process. The samples are post-deposition annealed in an N<sub>2</sub>

<sup>a)</sup>Author to whom correspondence should be addressed. Electronic mail: negulescu@univ-tours.fr.

atmosphere controlled oven at 265 °C and under specified magnetic field values. A Veeco Dimension 3100 magnetic force microscope is used to view the magnetic domains at zero field. A vibrating sample magnetometer with a temperature module allows the measurement of the macroscopic magnetic response of SAF samples as a function of applied field,  $M(H)$  curve, temperature, and angle. It especially allows the determination of the induced anisotropy axis. The model used to compute the  $M(H)$  curves of the multilayer is extensively developed in the Appendix. By fitting the experimental  $M(H)$  loops, the main parameters of the SAF structure can be extracted: the coupling energies, the anisotropy constants, and their thermal variations. Furthermore, the model gives access to the magnetization orientation of the two F layers with respect to the applied field as a function of temperature and field intensity. We will show that the model has a good predictive capacity that ensures the spin flop state necessary for linear field sensors.

### A. Spin flop with a SAF in its virgin state

First, we studied the magnetic properties of our SAFs in their virgin state. Since no magnetic field is applied during the deposition process, the magnetic properties of the as-deposited SAF structures have to be isotropic: the anisotropy axes of the AF IrMn layer are randomly distributed in all directions of space. This is confirmed at the macroscopic and microscopic scales. Indeed, the macroscopic  $M(H)$  curves are independent of the direction of the applied field in plane [Fig. 1(a)]. The microscopic MFM images taken on as deposited samples show a completely disordered magnetic state [Fig. 1(b)].

In order to investigate the exchange pinning process during the annealing procedure, the  $M(H)$  loop of the unbiased CoFe(1.5)/Ru(0.8)/CoFe(2.5) trilayer has to be measured at a temperature above 265 °C as shown in a previous study.<sup>9</sup>

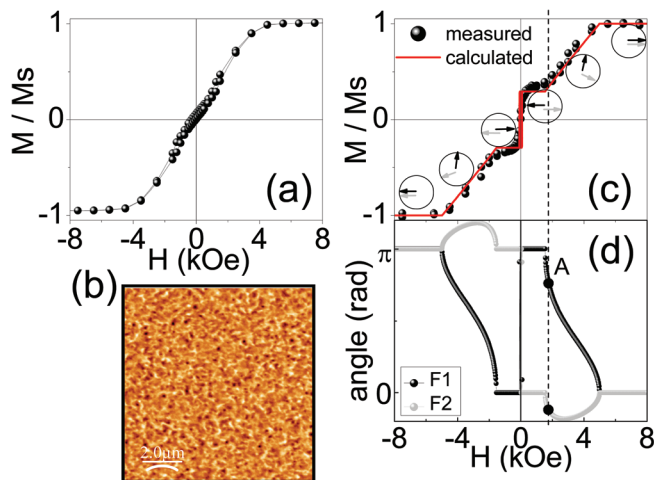


FIG. 1. (Color online) (a)  $M(H)$  curve for an as deposited sample measured at room temperature; (b) MFM image of the as deposited sample measured before any field cycling; (c)  $M(H)$  curve for the as deposited sample measured at 265 °C (filled black symbols). The red line represents the curve simulated using the model presented in the Appendix; (d) The calculated angles of the magnetization of both ferromagnetic layers, F1 and F2, with respect to the positive saturating field direction during the field cycling.

The  $M(H)$  loop shown in Fig. 1(c), measured at 265 °C, can then be fitted [continuous red line in Fig. 1(c)] using a macrospin model presented in the Appendix. The angles between the magnetizations of the two CoFe layers with respect to the direction of the applied field can be estimated from the model and are shown in Fig. 1(d). The magnetic orientation of the 1.5 nm thick CoFe layer, the F1 layer in our model, is of primary importance. Indeed, the 1.5 nm thick CoFe layer is in contact with the IrMn AF and its orientation will induce the pinning direction when the temperature is reduced below the blocking temperature of the IrMn film. If the applied field used for annealing is high enough to saturate the sample (a field higher than 5 kOe), the pinning direction should be parallel to the applied field. If a field lower than 1.5 kOe is used, the two CoFe films are in an antiparallel configuration and the pinning direction will be antiparallel to the total magnetization of the SAF. Between these two magnetic states, the SAF structure flops and its magnetization will be pinned in a direction that differs from the applied field direction.

In order to verify this analysis, the sample was annealed in a spin flop state for an applied field of 1.8 kOe [point A in Fig. 1(d)]. Then the  $M(H)$  loop of the annealed SAF is measured in a direction perpendicular to that of the annealing field. According to the macrospin model, the  $M(H)$  loop should be asymmetric and shifted due to the unidirectional anisotropy induced by the bias field. However, the resulting  $M(H)$  curve in Fig. 2(a) is symmetric and can be interpreted as a double shifted hysteresis loop resulting from the existence of two opposite pinning directions induced by the annealing procedure.<sup>6</sup> Since the spin flop state is prepared from a saturated magnetic state, two directions of magnetization rotation are

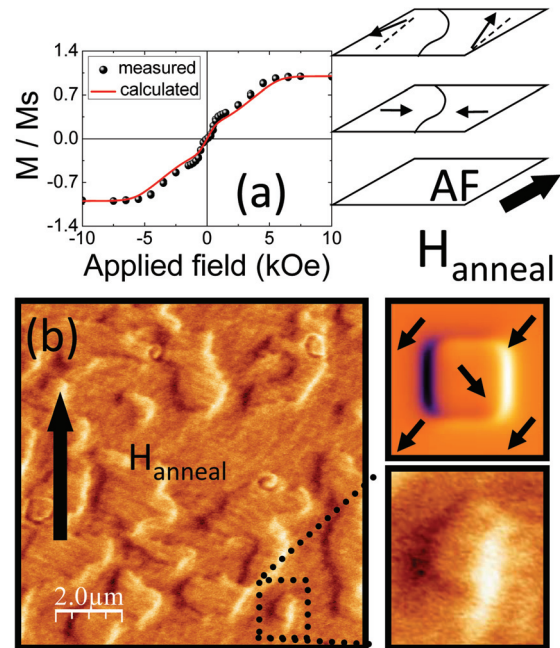


FIG. 2. (Color online) (a)  $M(H)$  curve measured at room temperature for a sample annealed in a field of 1.8 kOe (symbols) and the calculated curve obtained in a model that considers two domains of opposite anisotropies (red line); sketch of the magnetization distribution of F2 and F1 in contact with the AF layer; (b) MFM image showing domains of different orientations; magnified MFM image and calculation of the MFM contrast from the expected magnetization distribution.

energetically equivalent and the rotation direction of the magnetic moments cannot be controlled. As shown schematically in Fig. 2(a), clockwise and counterclockwise rotations can occur in adjacent regions of the sample leading to the formation of magnetic domains. These domains are then pinned during the field cooling procedure. At remanence, a nonuniform magnetization state should exist with domains. The shape of the cycle can be reproduced by our macrospin model taking this scenario into account. For the simulations, the sample is considered to be divided into two independent regions with different pinning directions. Starting from the fit of the  $M(H)$  cycle of a sample measured at high temperature [Fig. 1(c)], we can estimate the angle between the magnetization of the layer, F1, and the applied field at 1.8 kOe to be  $138^\circ$  [point A in Fig. 1(d)]. We have then considered that two types of domains are created in the sample, with pinning directions of  $\pm 138^\circ$  with respect to the annealing direction. The calculated  $M(H)$  curve for this magnetic structure is compared with the measured one in Fig. 2(a). We find a close agreement between simulation and experiment, with the calculated loop reproducing the double shifted experimental curve.

The presence of domains is confirmed by the MFM images [Fig. 2(b)]. The same domain configuration, two types of domains with pinning directions of  $\pm 138^\circ$  with respect to the annealing direction, has been used to calculate the MFM signal in order to interpret the observed contrast. Once again, in the magnified image, the contrasts are well reproduced by our model. In the magnified region, a domain with a pinning direction of  $+138^\circ$  is located in a bigger domain with a pinning direction of  $-138^\circ$ .

The first conclusion emerges from this study: we are not able to control the induced SF pinning direction in an isotropic sample. An anisotropy axis is required prior to the SF annealing procedure in order to break the initial symmetry and obtain a single domain state. Next, we will focus on the different possibilities to induce the anisotropy in the studied samples, aiming at identifying the optimum initial state of the SAF for a SF annealing process.

## B. The influence of anisotropy on the spin flop annealing process

An exchange anisotropy in the SAF can be obtained by either depositing the layers under a magnetic field or by post-deposition temperature annealing under applied field. In the first case, the magnetic fields that can be applied inside the deposition tools are, in general, on the order of some hundreds of Oe, which is far less than the saturation field of the SAF structure. The resulting exchange pinning anisotropies have been shown to be of poorer quality than those induced by high field annealing (see, for example, Ref. 14). In the second case, a high field that fully saturates the SAF structure is applied. Thus, well defined exchange pinning anisotropies are stabilized. In our case, the samples are deposited without an applied field. In order to reproduce the anisotropy obtained in a field deposition process, we performed a low field post-deposition annealing. The anisotropy acquired in this way is compared with the pinning obtained

after annealing in a saturating field. From Fig. 1(c) we know that: (i) for an annealing field of  $-250$  Oe, the two F layers are in an antiparallel state; (ii) at 13 kOe, the two F layers are oriented parallel to the direction of the field. In both cases, the annealing induces an exchange anisotropy axis parallel to the direction of the annealing field. This has been verified on the  $M(H)$  cycles measured after these 2 different annealing processes [Fig. 3(a)]. A plateau of the AP configuration of the two F layers is observed for both samples in a field ranging between  $-3000$  and  $+500$  Oe. The magnetization switching in low positive fields is hysteretic as shown in the inset of Fig. 3(a). Moreover, it can be seen that the sample annealed at low field shows more field hysteresis and a slightly increased slope of the AP plateau than the sample annealed in a saturating field. Apart from those small differences, the magnetization loops do not reveal detailed information about the anisotropy.

In order to differentiate the two annealing processes and to get the microscopic magnetic configurations, we investigated the magnetic state of the samples in zero field by MFM measurements. Notice that the remanent state now has two possible configurations: one corresponding to the AP plateau obtained when coming from negative fields and the second one with a smaller moment, obtained when coming from positive fields. Even if the differences in the total magnetic moments are quite small, the micromagnetic structures of these two states are extremely different, as can be observed from the MFM images presented in Figs. 3(b)–3(e). The images reported in Fig. 3(b) (high field annealing), and Fig. 3(d) (low field annealing) have been recorded after a saturation in a high positive field. They reveal the presence of  $360^\circ$  domain walls, as already reported in this type of structure.<sup>15,16</sup> According to the model, they appear during the reversal mechanism of the layer that is not in contact with the AF layer (i.e., F2) when the magnetic field is reduced to zero. These  $360^\circ$  domain walls are erased by applying a negative field in the easy axis (EA) direction [Figs. 3(c) and 3(e)], leaving room for rippled domain structures that are more pronounced for the sample annealed at low fields. Finally, while for the SAF annealed in high field the domain walls seem uniformly distributed over the whole surface of the sample, regions with and without domain walls are cohabitating in the other sample. The MFM contrasts have been reproduced for both annealing processes in the magnified images. The  $360^\circ$  domain walls (DWs) have been clearly identified. The main difference between the  $360^\circ$  DWs and the  $180^\circ$  ones is the presence of a double black/white contrast when the wall line is perpendicular to the magnetization direction. This figure allows us to confirm that the EA direction in the images Figs. 3(b) and 3(d) corresponds to the annealing field direction and that the structures observed by MFM are indeed  $360^\circ$  domain walls.

The magnetic state of the SAF structures annealed with two different applied magnetic fields ( $-250$  and 13 kOe) has to be analyzed more thoroughly in order to understand the differences between these two annealing processes. Indeed, an unsaturated magnetization state will induce exchange anisotropy distributions leading to differences in the anisotropies acquired during a high field and a low field annealing.



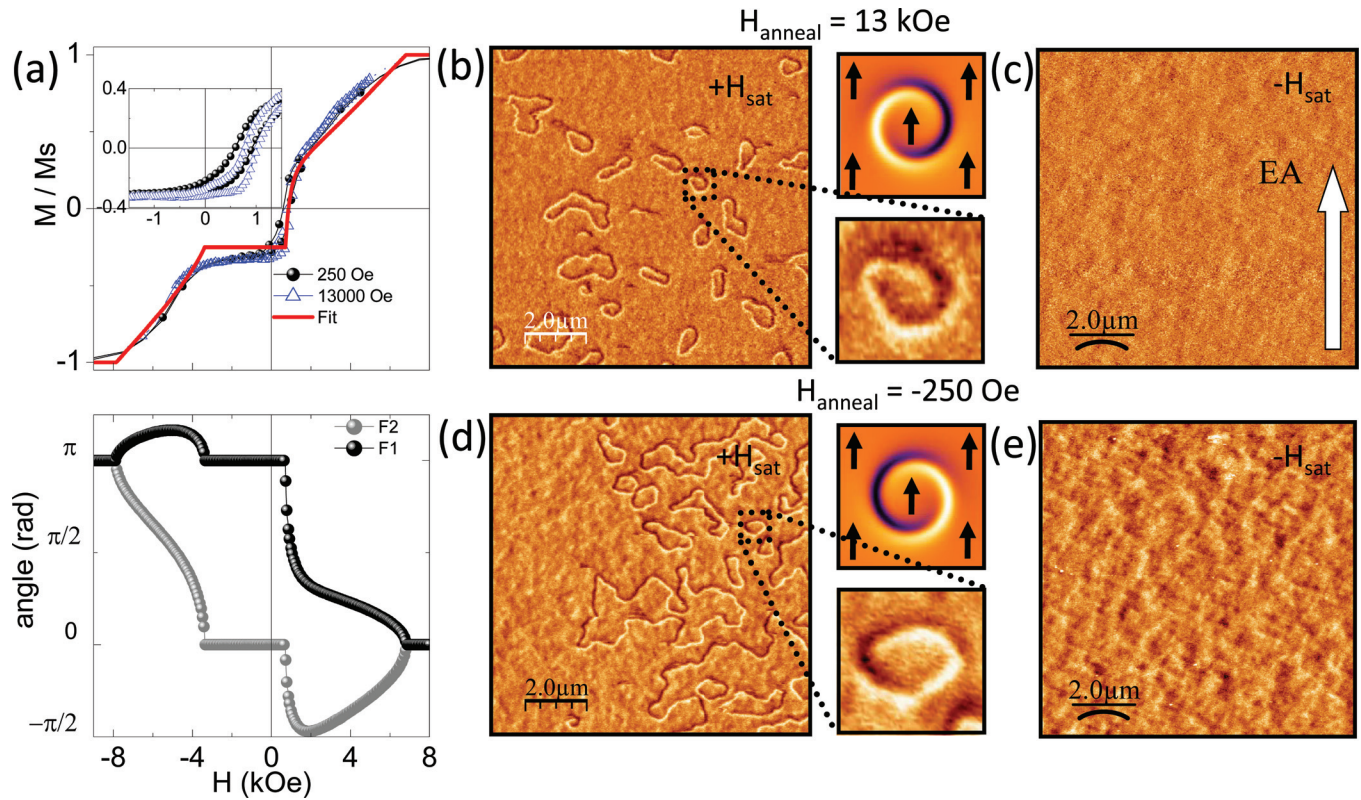


FIG. 3. (Color online) (a) Top:  $M(H)$  curves measured at room temperature for a sample annealed at  $-250$  Oe (filled black symbols) and a sample annealed at  $13$  kOe (blue empty symbols). The field is applied in the same direction as the annealing field. The red line is the result of the model presented in the Appendix. Bottom: magnetization angles of the two ferromagnetic layers of the SAF calculated from the model; (b) sample annealed at  $13$  kOe in MFM image obtained after applying a high positive field (positive and negative directions are identified with respect to the  $m(H)$  curves presented in (a)). The images at the right present a zoom of a circular  $360^\circ$  DW (down image) and the simulated DW structure (upper image); (c) MFM image obtained on the same sample after applying a high negative field. The zoomed image of a circular  $360^\circ$  DW is reproduced by simulation (upper image); (d) sample annealed at  $-250$  Oe: MFM image obtained after applying a high positive field; The zoomed image of a circular  $360^\circ$  DW is reproduced by simulation (upper image); (e) MFM image obtained on the same sample after applying a high negative field.

Quantitative information can be extracted from the hysteresis of the  $M(H)$  curves and from the ripple structure detected by the MFM images in the AP state.

First, we have analyzed the macroscopic  $M(H)$  curves and, as can be observed in the inset of Fig. 3(a), the exchange pinning field is slightly lower for the sample annealed in low field. We have studied the hysteretic properties as a function of the angle between the EA and the applied field direction. In order to estimate the hysteresis, the area enclosed between the ascending and the descending branches of the hysteresis cycle is calculated. The angular variation of the hysteresis for the two samples considered is presented in Fig. 4(a). While the sample annealed in low field shows a hysteresis that gradually decreases to zero in a range of  $25^\circ$  starting from the EA direction, a much faster reduction is obtained for the sample annealed in high field (in a range of  $10^\circ$ ). This evolution can be understood considering an angular distribution of the magnetization in the SAF structure. In this case, the angular distribution is larger for the low field annealing. As depicted in the high temperature curve in Fig. 1(a), at  $13$  kOe the SAF structure is saturated, while at  $-250$  Oe it does not present a clear AP orientation plateau. We can suppose that the magnetic moments of the two F layers are not perfectly aligned in the direction of the applied field for a value of  $-250$  Oe. This magnetic state is frozen during the field cooling process, giving rise to regions with slightly different

pinning orientations that can explain the coexistence of regions with and without  $360^\circ$  DWs.

Second, the magnetization fluctuations can also be inferred from the microscopic MFM images in Figs. 3(c) and 3(e). The ripples observed in the MFM measurements are analyzed using the 2 D auto correlation functions (ACFs). The profiles extracted from the autocorrelation images are qualitatively different for the two annealing processes [Fig. 4(b)]. In the case of the sample annealed in high field, the signal decreases quickly to zero, which is typical for an image

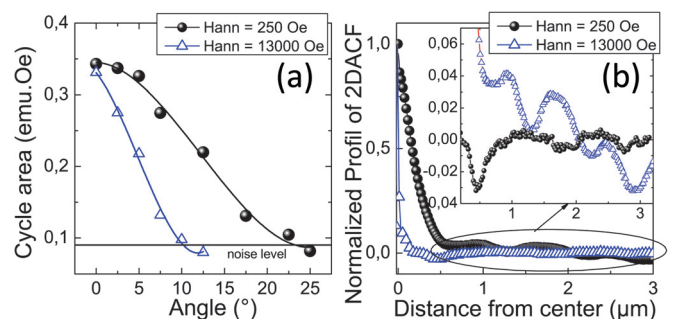


FIG. 4. (Color online) (a) Angular variation of the hysteresis area for two SAF structures annealed at  $-250$  Oe (circular black symbols) and at  $13$  kOe (triangular blue symbols); (b) profiles of the ACF made on the MFM ripple images for the same two samples. Inset: magnified ACF images showing the different behaviors.

without correlation. The structure annealed in low fields has a typical profile for ripples:<sup>17</sup> a slower decrease with an oscillating ACF signal that defines a characteristic correlation length of about  $0.6 \mu\text{m}$ . This means that applying a saturating field during the annealing process creates an exchange coupling anisotropy that exceeds the local anisotropies, making the appearance of ripples unfavorable. In contrast, when the annealing is done in low fields the induced exchange anisotropy does not overcome the local magnetocrystalline anisotropies. In this case a disordered state minimizes the total energy of the system, giving rise to the ripples observed in the MFM images. The suppression of the dispersion of magnetization in a ferromagnetic layer by exchange coupling was already revealed in bilayer systems.<sup>18</sup>

Since the coercivity cannot be correctly described by a coherent rotation model, we are not able to discriminate between the two magnetic states using the model described in the annex. However, in the literature we can find more complex models of exchange bias in polycrystalline samples<sup>19,20</sup> that take into account the variation of the EA directions in randomly oriented AF grains and irreversible transitions in the AF grains in order to describe coercivity. In a state where the thermal fluctuations can be neglected, the main source of coercivity comes from the inhomogeneous reversal of the F layer due to interactions with the AF grains which are supposed to have random anisotropy directions. The more disordered the AF system, the larger the distribution of the local pinning directions, leading to decreased values of exchange bias and broadening the angular variation of the hysteresis.

A second conclusion emerges from this study: after having investigated the different anisotropies induced by field annealing of the as deposited isotropic samples, it is clear that for a successful spin flop annealing process we need to control the rotation path of the magnetic moments. This can be achieved by exchange pinning the SAF structure prior to the spin flop annealing process. We conclude that the optimum initial state for a spin flop annealing process is the one given by a high field annealing, since it suppresses the magnetization dispersion in the ferromagnetic layers.

### C. Spin flop in SAF with a well-defined unidirectional anisotropy

A method to impose the magnetization's rotation direction consists of inducing a first order magnetic anisotropy axis in the SAF, exactly as it is done by imposing a unidirectional exchange anisotropy. Then, if a magnetic field is varied along a direction that is noncollinear with the exchange anisotropy axis, the magnetic moments are always rotating toward the pinning axis which minimizes the total energy of the system. This makes the magnetization reversal single domain, such as in a macrospin model. Therefore, as previously shown, it is necessary to anneal the samples under a high magnetic field to stabilize a well-defined exchange anisotropy axis. Consequently, a second annealing is necessary in the spin flop state using the following procedure. First, at room temperature, the sample is brought into a single domain state by applying a sequence of two magnetic fields: a saturation field that erases the eventual magnetic domains in

the sample, followed by the field value chosen for annealing. This second field will be sustained until the end of the process. At this point, the annealing process is started by increasing the temperature to  $265^\circ\text{C}$ . The system is kept at high temperature for 30 min and after that it is cooled to room temperature under a magnetic field. At high temperature, the initial exchange coupling between the F1 layer and the AF is erased and a new pinning direction is established, imposed by the magnetic orientation of the F1 layer during the cool down step.

The magnetic state of the F1 layer is controlled by two main parameters: the applied magnetic field and the coupling intensity between the two F layers. Regarding the influence of the applied field on the induced anisotropy we have to consider not only its value, but also its direction. Indeed, if the annealing for the spin flop is done with the field applied in the exchange pinning direction, once again the rotation direction of the magnetization cannot be controlled. This fact is illustrated by the MFM image of Fig. 5(b), where magnetic domains with opposite orientations are measured after such an annealing procedure. The field should be applied under an angle higher than the dispersion of the pinning directions fixed by the initial annealing, in order to avoid domain formation. In concordance with the angular variation of the hysteresis presented in the previous part [measurement from Fig. 4(a)], the critical angle is estimated to be less than  $10^\circ$ . This is indicated by the lack of domains in the MFM images obtained on samples re-annealed with a  $2.8 \text{ kOe}$  field applied at  $-10$  and  $+10^\circ$ .

To be sure to avoid the formation of domain walls in the F1 layer and always start from a single domain state, we choose to keep the direction of the field applied during the second annealing orthogonal to the initial anisotropy axis. The new exchange anisotropy axis is imposed by the magnetic orientation of the F1 layer that depends on the value of

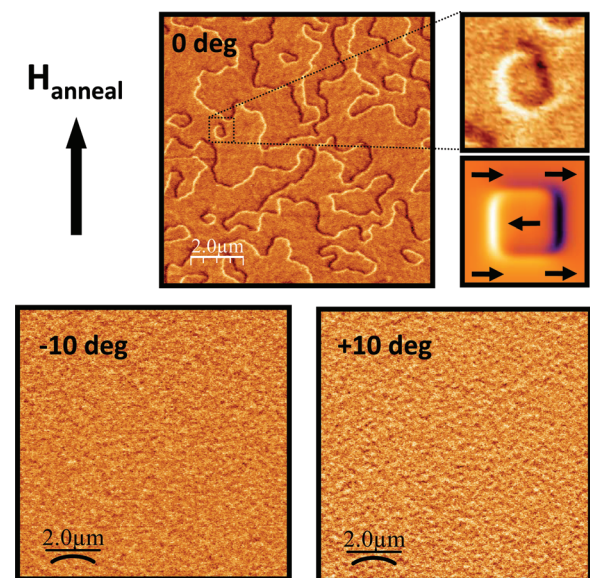


FIG. 5. (Color online) MFM images for 3 different samples annealed with the magnetic field applied under three different angles ( $-10^\circ$ ,  $0^\circ$ , and  $10^\circ$ ) with respect to the initial pinning direction. The magnified  $0^\circ$  field annealed sample image has been reproduced from the expected magnetization distribution.



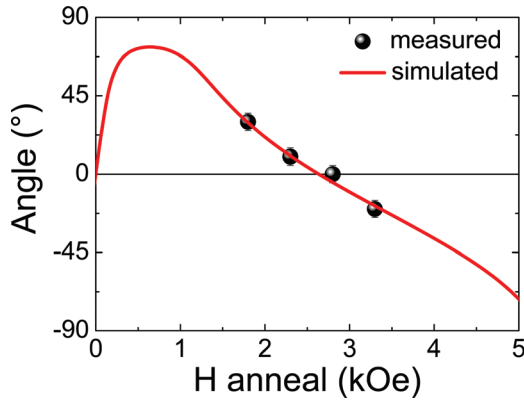


FIG. 6. (Color online) Angle of the pinning direction obtained after the spin flop annealing with the magnetic field applied orthogonal to the initial exchange anisotropy for different values of the annealing field. Scattered points are experimental data and the red line is simulated using the model described in the Appendix.

the annealing field. Therefore, by changing the value of the field applied during the annealing procedure, the direction of the pinning axis is modified. This dependence is depicted in Fig. 6, that represents the angular deviation of the new pinning direction from the initial one, as a function of the annealing field value. The experimental points are obtained from four different samples annealed under a field applied perpendicular to the initial exchange bias direction, with values ranging from 1.8 kOe to 3.3 kOe. The experimental data are compared with the calculated curve representing the angular variation of the magnetization of the F1 layer with the applied field. It is worth noting that this calculation is done without free parameters, and all quantities were extracted from previous experiences fitting the measured hysteresis loop at 250 °C. Very good agreement is found between the experimental measurements and the predicted dependence. This attests the good predictive capacity of the model we used.

#### D. Impact of the variation of $J_{\text{RKKY}}$ with temperature on the spin flop angle

Besides the annealing field intensity, another parameter that controls the spin flop direction is the Ruderman-Kittel-Kasuya-Yosida (RKKY) coupling between the two F layers across the Ru film. If this coupling varies with temperature, then the magnetic orientation of F1 of the SAF is expected to vary during the annealing process.

We have estimated the temperature variation of the SAF coupling constant by measuring the  $M(H)$  curves at different temperatures. The  $J_{\text{RKKY}}$  coupling energy is extracted by fitting the experimental data to the model proposed in the annex. The extracted values reported in Fig. 7(a) follow the theoretical variation predicted by Edwards *et al.*<sup>21</sup> and Bruno *et al.*<sup>22</sup>

$$J(T) = J_0(T/T_0)/\sinh(T/T_0), \quad (1)$$

where the characteristic temperature,  $T_0$ , is linked to the velocity of the electrons at the Fermi surface,  $v_F$ , and to the thickness of the Ru layer,  $t_{\text{Ru}}$

$$T_0 = (\hbar v_F)/(2\pi k_B t_{\text{Ru}}). \quad (2)$$

The parameters extracted from this fit,  $J_0 = -1.367 \text{ erg/cm}^2$  and  $T_0 = 240 \text{ K}$ , are in good agreement with the values obtained on an equivalent system (Co/Ru/Co).<sup>23</sup>

Due to the thermal variation of the  $J_{\text{RKKY}}$  coupling constant, the orientation of the SAF structure rotates during the cooling period of the annealing procedure if the applied field is kept constant. Figure 7(b) presents the angle of the F1 magnetization with respect to the applied field direction for different temperatures and an applied field of 2.8 kOe. If at high temperature the magnetic moments of the F1 layer are oriented perpendicular to the applied field, throughout the cool down step the magnetization rotates by more than 30°. So, for the studied process it seems relevant to identify the angle variation during the blocking of the SAF structure. In the annealing process, at a temperature denoted as  $T_B$  (blocking temperature), the AF should pin the adjacent SAF in the direction imposed by the F1 orientation at the considered temperature. Due to a dispersion of the AF grain volumes, a distribution of blocking temperatures is expected. Thus, during the cool down procedure different parts of the SAF should be pinned in slightly different directions. A pinning angle distribution can be expected from this annealing procedure, related to the blocking temperature distribution.

The blocking temperature ( $T_B$ ) distribution is determined by measuring the temperature variation of the exchange coupling at the F1/AF interface,  $J_{\text{ex}}$ . We chose to use the York protocol<sup>24</sup> consisting of the following procedure: the sample is kept at high temperature for 10 min at a field of 10 kOe in order to allow the reversal of the exchange pinning direction; afterwards the temperature is decreased to room temperature and the  $M(H)$  loop is measured; these two

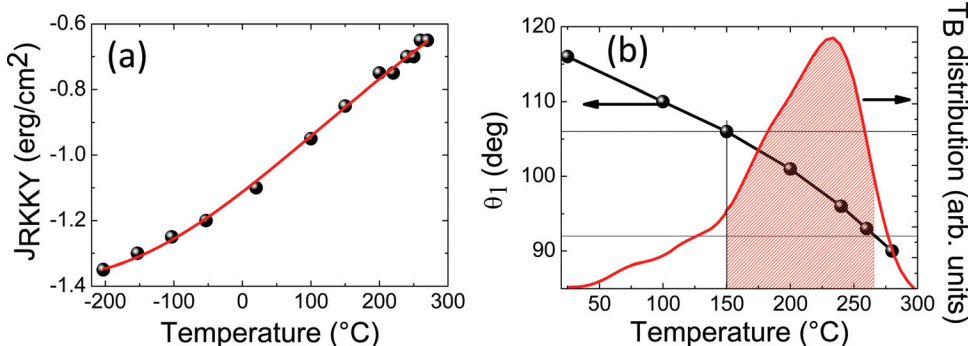


FIG. 7. (Color online) (a) Variation of the  $J_{\text{RKKY}}$  coupling constant with temperature; (b) calculated thermal variation of the angle,  $\theta_1$ , made by the magnetization of the F1 layer with the applied field direction (left) and the AF blocking temperature distribution.



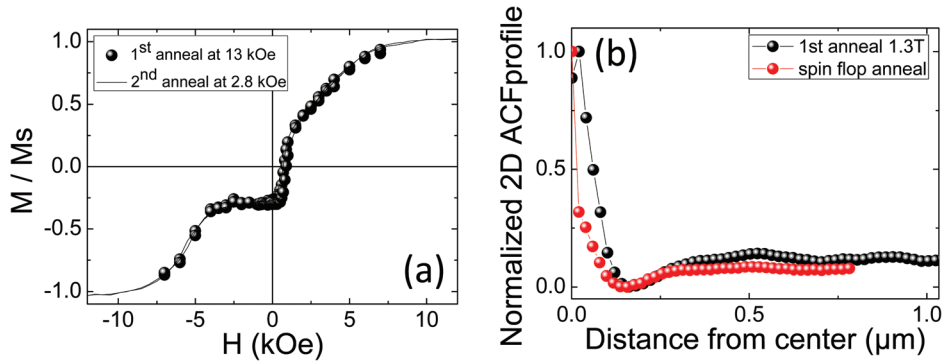


FIG. 8. (Color online) (a)  $M(H)$  curves measured on the same sample after a first anneal at 13 kOe and a second anneal at 2.8 kOe; (b) ACF profiles measured in the EA.

steps are repeated several times starting from a temperature of  $50^\circ\text{C}$  up to  $280^\circ\text{C}$ . The  $T_B$  distribution, defined as  $-dJ_{\text{ex}}/dT(T)$ , is presented in Fig. 7(b) and is plotted with the angular variation of the F1 magnetization. Let us consider that most of the sample is blocked in a temperature range extended from  $265^\circ\text{C}$  (the temperature used for annealing) down to  $150^\circ\text{C}$ . The corresponding rotation of the F1 magnetization is about  $16^\circ$ . As we explained before, the instability of the SAF magnetic orientation should induce a certain degree of disorder in the anisotropy induced by this annealing procedure. However, the experimental results do not reveal a dispersed orientation of the pinning directions. In Fig. 8(a) the hysteresis cycle of a sample which has been spin flop annealed is compared with the cycle measured before this annealing procedure. No differences in the hysteresis or the AP coupling plateaus are observed between the two  $M(H)$  curves. For a quantitative analysis, the micromagnetic states obtained by these different annealing procedures are analyzed using the ACF of the MFM images at remanence (images without  $360^\circ$  DW). Figure 8(b) presents the profiles of the two ACFs in the EA directions. The two curves are similar, showing a fast decrease to zero which is characteristic for the images without ripples. The same similarity between the two magnetic states is obtained when analyzing the angular variation of the hysteresis that shows a fast decrease to zero for a rotation of  $10^\circ$  between the applied field direction and the exchange anisotropy direction. The equivalence between the anisotropies induced by these two different annealing procedures indicates that the angular distribution of the pinning directions induced by spin flop annealing does not introduce more disorder in the AF system than the one given by the intrinsic dispersion of the AF magnetocrystalline anisotropies.

### E. Application in linear MR devices

In order to test the predictive capacity of the model and to demonstrate the usefulness of both the model and the presented procedure for applications, we have used the model with measurements made on samples designed for magnetic sensing application (i.e., having a linear magnetoresistive response in the low field range). The spin flop procedure was used on a spin valve system to induce an orthogonal pinning between a detection layer (DL) composed of a CoFe 5/IrMn 7 stack and the studied pinned SAF structure used as

reference electrode. A first thermal annealing at  $265^\circ\text{C}$  and in high field is used to pin both the reference and the detection electrodes parallel to the direction of the applied field. A second thermal annealing is done at the same temperature, but with the field applied perpendicular to the initially established anisotropy direction. During this second annealing procedure the DL is oriented parallel to the annealing field direction, indicating that its pinning direction rotates perpendicular to the initial exchange anisotropy axis. By choosing the value of the annealing field in the range where the SAF structure flops, the pinning direction of the SAF can be tuned perpendicular to the field. The magnetoresistive (MR) characteristics of the spin valves are measured using a homemade 4 point electric prober.

Figure 9(a) presents the MR curves measured for three samples annealed in the spin flop state, for three different annealing fields. In the low field range, a linear variation of the MR is observed as a result of the crossed anisotropies induced in the detection and reference electrodes. The pinning angle of the SAF varies as a function of the annealing field value, in concordance with the result presented in Fig. 6. As a result, the shape of the MR(H) curves varies as a function of the annealing conditions: the linear variation is shifted upward with an increased value of the annealing field and the maximum MR value is achieved only when arriving

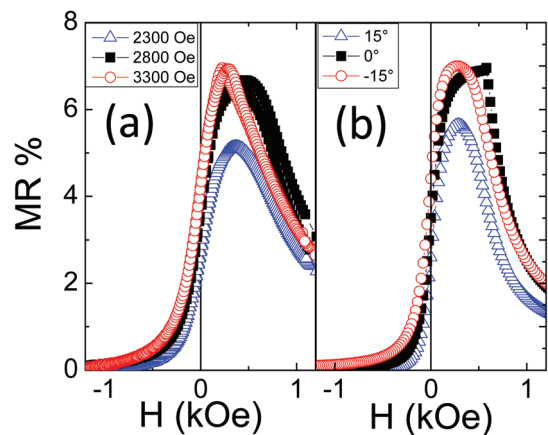


FIG. 9. (Color online) (a) MR(H) curves measured on 3 spin valves annealed at different applied fields; (b) simulated MR(H) curves for the three different spin flop angles associated with the three annealing fields.

at the perpendicular orientation between the SAF and the DL. In order to analyze the experimental curves, MR(H) variations were simulated using the angles of the pinning direction of the reference SAF structure predicted by the theoretical model. The MR of this device can be written as,

$$\text{MR} = \frac{R_{\min} + R_{\max}}{2} + \frac{R_{\min} - R_{\max}}{2} \cos(\varphi), \quad (3)$$

where  $\varphi$  is the angle between the magnetization of the detection layer and the orientation of the reference SAF. For a pinned detection layer, this angle can be calculated as,<sup>25</sup>

$$\varphi = \frac{\pi}{2} - \arctan\left(\frac{H}{H_{\text{ex}}^{\text{DL}}}\right) + \theta_2, \quad (4)$$

with  $H_{\text{ex}}^{\text{DL}}$  as the exchange field of the DL and  $\theta_2$  as the angle between the magnetization of the F<sub>2</sub> layer in the SAF and the applied field direction. The measured value of the DL exchange field is  $H_{\text{ex}}^{\text{DL}} = 135$  Oe. The value of  $\theta_2$  is obtained from the theoretical model, after imposing a certain pinning direction of the SAF. From the previous section (see Fig. 6) we know how the pinning direction of the SAF structure is related to the field used during the spin flop annealing process.

The simulated MR(H) curves are presented in Fig. 9(b). Very good agreement is found between the experimental measurements and the MR response predicted by the model. This allows us to precisely analyze the experimental curves. When the spin flop annealing is done in a field ensuring the orthogonal orientation (zero spin flop angle), the SAF has a stable AP state in the linear range of the device. In this magnetic orientation, the linear MR signal is given only by the rotation of the detection layer magnetization. For different annealing field values, the plateau of the AP orientation of the SAF is quickly disappearing. If the pinning angle of the SAF is positive, the F2 magnetization rotates toward the exchange anisotropy direction, indicating that the angle between the magnetizations of the detection and the reference layers will increase. From Eqs. (3) and (4), this orientation leads to a reduced MR signal in the low field range. The maximum MR value is no longer achieved. Inversely, when the pinning angle of the SAF is negative, the magnetization of the F2 layer rotates toward the detection layer. The MR signal is therefore increased for lower field values. The maximum MR value is achieved, but the lack of magnetic rigidity in the SAF reference electrode is reflected in the reduced field range of the high resistance state.

### III. CONCLUSIONS

A systematic study of the annealing induced anisotropies in a pinned SAF has been shown at the macroscopic and microscopic levels. The annealing in a spin flop state of the SAF structure is analyzed as a function of the annealing field value and direction. It is shown that the temperature variation of the RKKY coupling constant during the annealing process does not modify the exchange anisotropy axis, which seems to be established at high temperature. Using a

macrospin model with parameters depending on temperature we are able to predict the pinning direction obtained through a spin flop annealing process. This model is used to interpret the MR curves measured on a spin valve system with crossed anisotropies obtained by such an annealing process.

### ACKNOWLEDGMENTS

This work was partially financed by the ANR CAMEL and SPINCHAT projects.

### APPENDIX: ANALYSIS OF EXPERIMENTAL RESULTS

A macrospin model is used to analyze the experimental results. The model supposes two F layers coupled by a coupling constant,  $J_{\text{RKKY}}$ . The two F layers are characterized by their anisotropy constant,  $K_F$ , their saturation magnetization,  $M_S$ , and their thicknesses,  $t_1$  and  $t_2$ . One of the two F layers is coupled to an AF layer by an exchange coupling constant  $J_{\text{ex}}$ . The total energy per unit surface of the studied system can be expressed as

$$\begin{aligned} E = & K_F t_1 \sin^2(\theta_1) + K_F t_2 \sin^2(\theta_2) - J_{\text{RKKY}} \cos(\theta_1 - \theta_2) \\ & - H [M_S t_1 \cos(\alpha - \theta_1) + M_S t_2 \cos(\alpha - \theta_2)] \\ & - J_{\text{ex}} \cos(\beta - \theta_1). \end{aligned} \quad (\text{A1})$$

The first two terms in Eq. (A1) describe the anisotropy of the two F layers. The third term corresponds to the coupling between the two F layers of the SAF, while the next one is the Zeeman energy of both layers. Here,  $\alpha$  is the angle between the applied field,  $H$ , and the anisotropy direction. Finally, the last term of the total energy represents the exchange coupling between the AF and F1, where  $\beta$  is the angle between the pinning direction and the anisotropy of the F layers, and  $\theta_1$  and  $\theta_2$  are the angles between the magnetization of the two F layers and the direction of the anisotropy. The magnetic state of the SAF system can be obtained by a minimization of the energy as a function of  $\theta_1$  and  $\theta_2$ .

The thicknesses of the two F layers are taken equal with the experimental nominal ones:  $t_1 = 1.5$  nm and  $t_2 = 2.5$  nm. The value of  $K_F$  is considered equal to  $2 \times 10^4$  erg/cm<sup>3</sup> and  $M_S = 1600$  emu/cm<sup>3</sup>. The values of  $t_1$ ,  $t_2$ , and  $M_S$  are adjusting the magnetization amplitude of the antiparallel plateau. In the model, we kept the values of the two thicknesses equal with the experimental nominal thicknesses and we slightly varied the  $M_S$  value in order to simulate the experimental M(H) curves. With these four parameters defined, the values of the coupling constants,  $J_{\text{ex}}$  and  $J_{\text{RKKY}}$ , are obtained by fitting the experimental M(H) curves. At room temperature,  $J_{\text{RKKY}} = -1.1$  erg/cm<sup>2</sup> and  $J_{\text{ex}} = 0.18$  erg/cm<sup>2</sup>. Both coupling constants decrease with increased temperature and at 265 °C,  $J_{\text{ex}}$  is zero while  $J_{\text{RKKY}} = -0.65$  erg/cm<sup>2</sup>. The value of  $K_F$  does not play a significant role in this model. The ferromagnetic anisotropy  $K_F \times t_F \approx 8 \times 10^{-3}$  erg/cm<sup>2</sup> is two orders of magnitude lower than the RKKY coupling energy and almost 3 orders of magnitude lower than the Zeeman term in saturating fields.

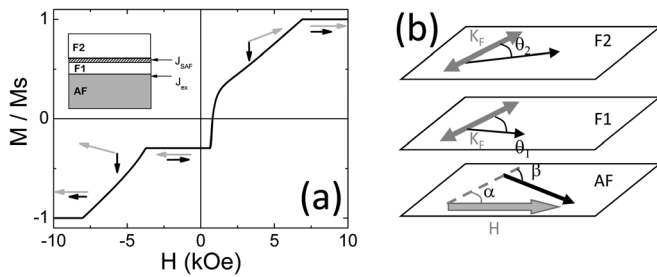


FIG. 10. (a)  $M(H)$  curve calculated from the model presented in the Appendix. Inset: the multilayer structure with the two ferromagnetic layers, F1 and F2; (b) sketch of the multilayer stack with the definition of the angles involved in the model.

The simulated  $M(H)$  curve at room temperature is represented in Fig. 10. The arrows represent the orientation of the two F layers for different field values. At low field, the RKKY coupling is predominant and the system has an antiparallel configuration. When the applied field is increased, the antiparallel coupling of the two F layers is no longer favorable and the layers rotate parallel with the field, passing through a state where both are not collinear with the applied field. This is called the spin flop state.

<sup>1</sup>H. A. M. van der Berg, W. Clemens, G. Gieres, G. Rupp, W. Schelter, and M. Vieth, *IEEE Trans. Magn.* **32**, 4624 (1996).

<sup>2</sup>J. L. Leal and M. H. Kryder, *J. Appl. Phys.* **83**, 3720 (1998).

<sup>3</sup>J. G. Zhu and Y. Zheng, *IEEE Trans. Magn.* **34**, 1063 (1998).

<sup>4</sup>J. G. Zhu, *IEEE Trans. Magn.* **35**, 655 (1999).

<sup>5</sup>H. C. Tong, C. Qian, L. Miloslavsky, S. Funada, X. Shi, F. Liu, and S. Dey, *J. Appl. Phys.* **87**, 5055 (2000).

<sup>6</sup>R. S. Beach, J. McCord, P. Webb, and D. Mauri, *Appl. Phys. Lett.* **80**, 4576 (2002).

<sup>7</sup>Z. Q. Lu and G. Pan, *Appl. Phys. Lett.* **82**, 4107 (2003).

<sup>8</sup>C. H. Tsang, R. E. Fontana, T. Lin, D. E. Heim, B. A. Gurney, and M. L. Williams, *IBM J. Res. Dev.* **42**, 103 (1998).

<sup>9</sup>B. Negulescu, D. Lacour, F. Montaigne, A. Gerken, J. Paul, V. Spetter, J. Marien, C. Duret, and M. Hehn, *Appl. Phys. Lett.* **95**, 112502 (2009).

<sup>10</sup>C. H. Marrows, F. E. Stanley, and B. J. Hickey, *J. Appl. Phys.* **87**, 5058 (2000).

<sup>11</sup>Y. R. Uhm, K. H. Shin, and S. H. Lim, *J. Appl. Phys.* **91**, 6929 (2002).

<sup>12</sup>Z. Lu, G. Pan, A. Al-Jibouri, and M. Hoban, *J. Appl. Phys.* **91**, 7116 (2002).

<sup>13</sup>S. H. Jang, T. Kang, H. J. Kim, and K. Y. Kim, *J. Magn. Magn. Mater.* **239**, 179 (2002).

<sup>14</sup>H. Li, P. P. Freitas, Z. Wang, J. B. Sousa, P. Gogol, and J. Chapman, *J. Appl. Phys.* **89**, 6904 (2001).

<sup>15</sup>H. Boeve, L. Esparbe, G. Gieres, L. Bär, J. Wecker, and H. Brückl, *J. Appl. Phys.* **91**, 7962 (2002).

<sup>16</sup>C. Tiusan, T. Dimopoulos, K. Ounadjela, M. Hehn, H. A. M. van den Berg, V. da Costa, and Y. Henry, *Phys. Rev. B* **61**, 580 (2000).

<sup>17</sup>D. V. Berkov and N. L. Gorn, *Phys. Rev. B* **57**, 14332 (1998).

<sup>18</sup>M. Ali, C. H. Marrows, B. J. Hickey, F. Offi, J. Wang, L. I. Chelaru, M. Kotsugi, and W. Kuch, *Phys. Rev. B* **79**, 064415 (2009).

<sup>19</sup>G. Scholten, K. D. Usadel, and U. Nowak, *Phys. Rev. B* **71**, 064413 (2005).

<sup>20</sup>M. D. Stiles and R. D. McMichael, *Phys. Rev. B* **63**, 064405 (2001).

<sup>21</sup>D. M. Edwards, J. Mathon, R. B. Muniz, and M. S. Phan, *Phys. Rev. Lett.* **67**, 493 (1991).

<sup>22</sup>P. Bruno and C. Chappert, *Phys. Rev. Lett.* **67**, 1602 (1991).

<sup>23</sup>Z. Zhang, L. Zhou, P. E. Wigen, and K. Ounadjela, *Phys. Rev. B* **50**, 6094 (1994).

<sup>24</sup>L. E. Fernandez-Outon, K. O'Grady, and M. J. Carey, *J. Appl. Phys.* **95**, 6852 (2004).

<sup>25</sup>G. Malinowski, M. Hehn, M. Sajieddine, F. Montaigne, E. Jouguelet, F. Canet, M. Alnot, D. Lacour, and A. Schuhl, *Appl. Phys. Lett.* **83**, 4372 (2003).